

Tight-binding g Factor Calculations of CdSe Nanostructures

Joshua Schrier and K. Birgitta Whaley

Department of Chemistry and Pitzer Center for Theoretical Chemistry, University of California, Berkeley 94720

The Lande g factors for CdSe quantum dots and rods are investigated within the framework of the semiempirical tight-binding method. We describe methods for treating both the n -doped and neutral nanostructures, and then apply these to a selection of nanocrystals of variable size and shape, focusing on approximately spherical dots and rods of differing aspect ratio. For the negatively charged n -doped systems, we observe that the g factors for near-spherical CdSe dots are approximately independent of size, but show strong shape dependence as one axis of the quantum dot is extended to form rod-like structures. In particular, there is a discontinuity in the magnitude of g factor and a transition from anisotropic to isotropic g factor tensor at aspect ratio ~ 1.3 . For the neutral systems, we analyze the electron g factor of both the conduction and valence band electrons. We find that the behavior of the electron g factor in the neutral nanocrystals is generally similar to that in the n -doped case, showing the same strong shape dependence and discontinuity in magnitude and anisotropy. In smaller systems the g factor value is dependent on the details of the surface model. Comparison with recent measurements of g factors for CdSe nanocrystals suggests that the shape dependent transition may be responsible for the observations of anomalous numbers of g factors at certain nanocrystal sizes.

I. INTRODUCTION

The electronic structure and linear optical spectroscopy of semiconductor nanocrystals have been the subject of considerable theoretical attention over the last ten years. The size scaling of excitonic absorptions, excitonic fine structure, and role of atomistic effects such as surface reconstruction, are relatively well understood. Less is known about the behavior of the electronic states in the presence of a magnetic field. Recent experimental demonstrations of long-lived spin coherences in semiconductor nanostructures¹ have provided motivation for a detailed fundamental investigation of the behavior of electronic excitations in magnetic fields. The spin lifetimes appear to be longest in nanostructures possessing full three-dimensional confinement, namely quantum dots, where undoped nanocrystals show room temperature spin lifetimes of up to 3 ns,² considerably larger than the corresponding lifetimes for undoped quantum wells and bulk semiconductors (~ 50 psec - 1 nsec).¹ Since lifetimes are typically significantly increased by doping, quantum dots show considerable potential for optimizing long-lived spin degrees of freedom.³

Despite this experimental promise, to date even the basic magneto-optical phenomena in these nanostructures are not well understood theoretically. Thus, one unexplained phenomenon in the study of semiconductor nanocrystals (NC's) is the appearance of multiple Lande g factors in CdSe quantum dots (QD's). Time Resolved Faraday Rotation (TRFR) studies of excitons in CdSe QD's reveal multiple g factors for certain dot sizes, with either two or four values detected.^{2,4,5} However, magnetic circular dichroism (MCD) measurements apparently reveal a single g factor per exciton state in the two dot sizes studied (19 Å and 25 Å diameter).⁶ As noted in Ref. 2, the Faraday rotation in neutral quantum dots should contain signatures of both electron and hole spins, with the relative contributions determined by the detailed coupling between these in the excitonic state. However there is currently no real understanding of why more than one g factor should be observed in TRFR, nor why for one particular size four values are detectable. Some investigators have conjectured that multiple g factors may result from excitonic fine structure in the QD energy levels, reflecting the fact that different fine structure levels would be expected to possess different excitonic g factors.⁶ The bright and dark exciton states for CdSe have been predicted to possess quite different excitonic g factor values. However fits to magnetic field-dependent polarization-resolved photoluminescence spectra to extract the g values for the dark exciton states⁷ do not show agreement with corresponding measurements from circular dichroism.⁶ Moreover, TRFR measurements with excitation energies tuned to different excitonic fine structure states do not appear to show different g factors.² Others have proposed that both the electron and exciton signatures may all be present in TRFR,² or that multiple values arise from an electronic contribution coexisting with an exciton contribution within an ensemble of QDs.⁴ Comparison of values extracted from MCD and from TRFR is not straightforward; whereas the effective mass treatment of MCD experiments calculates the exciton g factor from a constant electron contribution and a calculated hole g factor,⁶ the treatment of what is hypothesized to be an exciton g factor in TRFR experiments is obtained using a calculated electron contribution and uses a fixed hole g factor.⁴

Theoretical analysis is complicated by the possible contributions of crystal symmetry induced anisotropy in the hole g factor, by the effects of exchange coupling in exciton states, as well as by the possible effects of nanocrystal shape and surface contributions. Conversely, experimental efforts to assign the multiple g factors observed are complicated by the use of a distribution of randomly oriented nanocrystals having non-uniform size and shape. Efforts to average

anisotropy that might arise in a TRFR-measured exciton g factor as a result of anisotropy of the hole g factor in a hexagonal crystal over an ensemble of randomly oriented QDs do not show qualitative agreement with experiment.⁵ A recent proposal based on effective mass analysis has suggested that exciton precession is exhibited only by a special subset of the QD ensemble, termed ‘quasi-spherical’, in which there is an effective cancellation between the intrinsic anisotropy due to the hexagonal structure and that due to the nanocrystal shape, and resulting in isotropic g factors, while all other shape QDs presumed to exhibit only electron precession.⁴ We shall term this the isotropically quasi-spherical region, since no explicit aspect ratio range is proposed and the use of the term ‘spherical’ refers only to the three-fold degeneracy of the g tensor components. This regime is to be distinguished from the geometrically quasi-spherical region in which the QDs have aspect ratios near unity. In general, the isotropically and geometrically quasi-spherical regimes may or may not be coincident.

In this work we investigate the g factors of CdSe nanostructures within the framework of semiempirical tight-binding. Unlike effective mass treatments,⁸ this has the advantage of retaining the atomistic nature of the problem, and thereby allowing for realistic treatment of ligand and reconstruction effects at the surface.⁹ Since it is possible to synthesize a wide variety of CdSe nanostructures, such as rods and tetrapods, in a controlled fashion,¹⁰ it is useful to have a theory which may be applied to arbitrary structures. To demonstrate this point, we describe here calculations for both CdSe dots and for rods of variable aspect ratio. Additionally, it is possible to create electrically n -doped dots,^{11,12} although the g factors for these systems have not yet been experimentally determined. To a first approximation, the n -doped electron g factors will be equivalent to those of an electron in the conduction band. In light of this, we describe here theoretical treatments for both n -doped and excitonic systems. We have endeavored to use only tight-binding parameters applied previously in the literature to treat other properties. In particular, we employ a tight-binding description that was augmented for linear optical properties.¹³ We note that while this use of a parameterization that has not been optimized specifically for magneto-optical properties may limit our ability to obtain quantitatively accurate results, the qualitative physical behavior should nevertheless give us an understanding of the effects of NC size and shape on the anisotropy of the g tensor. The calculations in this paper employ tight-binding models of nanocrystals possessing unreconstructed surfaces, using realistic models of surface passivation developed previously.^{9,13,14} The modifications that might be induced by surface reconstruction will be briefly discussed in the context of calibration calculations made with truncated surfaces.

II. THEORY

A. Single particle Hamiltonian

The effective single-particle Hamiltonian is calculated with the nearest-neighbor sp^3s^* basis tight-binding approach, using the standard semiempirical matrix elements,¹⁵ transformed from zinc blende to hexagonal crystal structure according to the transformations given in Ref. 9. Numerical diagonalization yields the single particle states, $\psi_i(\mathbf{r}_i)$, and single particle energies, E_i for a given state i .

B. g tensor for a single electron in the conduction level

The derivation of the g factor in finite molecular systems is conducted by equating the phenomenological spin Hamiltonian,

$$H_{phenom} = \mu_B \mathbf{B} \cdot \mathbf{g} \cdot \mathbf{s}, \quad (1)$$

(where μ_B is the Bohr magneton, \mathbf{B} is the magnetic field vector, \mathbf{g} is the so-called g tensor, and \mathbf{s} is the spin-vector), with the theoretical spin Hamiltonian

$$H_{spin} = g_0 \mu_B \mathbf{s} \cdot \mathbf{B} + \xi \mathbf{l} \cdot \mathbf{s} + \mu_B \mathbf{l} \cdot \mathbf{B}. \quad (2)$$

Here g_0 is the free-electron g factor, ξ is the spin-orbit coupling, and \mathbf{l} is the orbital-angular momentum operator). We have neglected the contribution of hyperfine interactions here. This spin Hamiltonian H_{spin} containing all magnetic field and spin-orbit coupling terms, is to be added to a spatial Hamiltonian, H_0 , that is evaluated here within tight-binding.¹⁵

Our method for calculating the g tensors of n -doped systems follows the theoretical treatment made for finite molecular systems by Stone, which treats H_{spin} as a second order perturbation.¹⁶ Similar Extended Hückel treatments of organometallic compounds¹⁷ and small radicals¹⁸ have also been reported. The g tensor for a doublet radical,

corresponding to a single unpaired electron spin, is given by

$$g_{ij} = g_0 \delta_{ij} + 2 \sum_{k, n \neq 0} \frac{\langle \psi_0 | \xi_k(r_k) \mathbf{I}_k^i | \psi_n \rangle \langle \psi_n | \mathbf{I}_k^j | \psi_0 \rangle}{E_0 - E_n}, \quad (3)$$

where $\{i, j\}$ are Cartesian components, g_0 is the free electron g factor, ψ_0 denotes the single-particle eigenvector corresponding to the unpaired electron state, n runs over all of the doubly-occupied and virtual orbitals, $\xi_k(r_k)$ is the spin-orbit coupling as a function of r_k , and \mathbf{I}_k^i is the orbital angular momentum operator component in the i th Cartesian direction centered on the k th atom. We assume that the additional doping electron can simply be placed in the lowest unoccupied molecular orbital that is derived from the single-particle calculation. We have also neglected the gauge-correction term,¹⁶ e.g., for g_{zz} ,

$$\frac{m}{\hbar^2} \langle \psi_0 | \sum_k (x_k^2 + y_k^2) \xi_k(r_k) | \psi_0 \rangle. \quad (4)$$

This is justified since both Stone's analysis and our own preliminary calculations indicate that the magnitude of this term is small. However, as discussed at the end of this section, as well as in Section IV B, our estimation of this term is dependent on the magnitude of the transition dipole matrix elements, and hence dependent on the parameterization of these values.

We expand the n -th single-particle state in terms of the basis of atomic orbitals at the k site,

$$|\psi_n\rangle = \sum_k \left| \chi_{(k)}^{(n)} \right\rangle = \sum_k \left\{ c_{(s,k)}^{(n)} |s, k\rangle + c_{(p_x,k)}^{(n)} |p_x, k\rangle + c_{(p_y,k)}^{(n)} |p_y, k\rangle + c_{(p_z,k)}^{(n)} |p_z, k\rangle + c_{(s^*,k)}^{(n)} |s^*, k\rangle \right\}. \quad (5)$$

Here the ket form of $\chi_{(k)}^{(n)}$ is to be understood as consisting of all the atomic ($\{sp^3s^*\}$) orbitals on site k , with coefficients included according to the expression in Eq. (5). We now introduce two approximations to simplify the evaluation of the spin-orbit coupling and orbital angular momentum matrix elements in Eq.(3), following Stone.¹⁶ First, since the spin-orbit coupling is $\xi(r) \sim r^{-3}$, then $\xi_k(r_k)$ is effectively zero except near atom k , and thus

$$\langle \psi_0 | \xi_k(r_k) \mathbf{I}_k^i | \psi_n \rangle \approx \left\langle \chi_{(k)}^{(0)} \left| \xi_k(r_k) \mathbf{I}_k^i \right| \chi_{(k)}^{(n)} \right\rangle \approx \xi_k \left\langle \chi_{(k)}^{(0)} \left| \mathbf{I}_k^i \right| \chi_{(k)}^{(n)} \right\rangle, \quad (6)$$

where ξ_k is the spin-orbit coupling constant for atom k , which has been parameterized for semiconductor systems by Chadi:¹⁹ $\xi_{Cd} = 0.151$ eV, $\xi_{Se} = 0.32$ eV. Since, in our current model for CdSe, the oxygen ligands are modeled as consisting of an s -orbital only,¹³ they contribute no spin-orbit coupling. This may be justified by noting that $\xi_O = 0.0187$ eV is an order of magnitude smaller than ξ_{Cd} .²⁰ Second, for the orbital angular momentum matrix element,

$$\langle \psi_n | \mathbf{I}_k^j | \psi_0 \rangle = \sum_{k', k''} \left\langle \chi_{(k')}^{(n)} \left| \mathbf{I}_k^j \right| \chi_{(k'')}^{(0)} \right\rangle, \quad (7)$$

using the relation $l_k = l_{k'} + \hbar^{-1} \mathbf{r}_{kk'} \times \mathbf{p}$. Assuming that the atomic orbitals are approximate eigenfunctions of parity, we can show that for Eq.(6) not to vanish, the matrix elements of \mathbf{p} must vanish. In addition, a tight-binding treatment assumes that overlap between orbitals on different atoms is zero, leading to

$$\langle \psi_n | \mathbf{I}_k^j | \psi_0 \rangle \approx \sum_{k'} \left\langle \chi_{(k')}^{(n)} \left| \mathbf{I}_{k'}^j \right| \chi_{(k')}^{(0)} \right\rangle. \quad (8)$$

Combining these two approximations, Eq.(3) becomes

$$g_{ij} = g_0 \delta_{ij} + 2 \sum_{n \neq 0} \frac{\left(\sum_k \xi_k \left\langle \chi_{(k)}^{(0)} \left| \mathbf{I}_k^i \right| \chi_{(k)}^{(n)} \right\rangle \right) \left(\sum_{k'} \left\langle \chi_{(k')}^{(n)} \left| \mathbf{I}_{k'}^j \right| \chi_{(k')}^{(0)} \right\rangle \right)}{E_0 - E_n}. \quad (9)$$

We have used $|E_0 - E_n| < 0.05$ meV as the criterion for degeneracy in the calculations reported here.

Though the first approximation, Eqs. (6) - (7), is quite reasonable, one might question the validity of the second approximation, Eq.(8). Indeed, in semiempirical Intermediate Neglect of Differential Overlap (INDO) type calculations,^{21,22,23} it has been found numerically that this is not a good approximation. For the general element $\left\langle \chi_{(k)}^{(0)} \left| \mathbf{I}_k^i \right| \chi_{(k'')}^{(0)} \right\rangle$, there are five different equality or nonequality relations between k , k' , and k'' (i.e., $k = k' = k''$,

$k = k' \neq k'', k = k'' \neq k', k' = k'' \neq k, k \neq k' \neq k''$). Evaluating these in the atomic basis, using the relations $l_k = l_{k'} + \hbar^{-1} \mathbf{r}_{kk'} \times \mathbf{p}$ and $p_\alpha = im_e \hbar^{-1} [H, \alpha]$, and taking the overlap between orbitals on different atoms as zero (which is an assumption of the tight-binding formalism itself and not introduced in our derivation), then the correction term that must be added to the α component (α, β, γ Cartesian components) of Eq.(8) is

$$\sum_{k' \in nn(k)} \sum_{\substack{k'' \in nn(k) \\ k'' \neq k'}} \epsilon_{\alpha\beta\gamma} \left(\frac{m_e}{i\hbar^2} \right) r_{kk''}^{(\beta)} \langle \chi_{(k')}^{(n)} | [r^{(\gamma)}, H_0] | \chi_{(k)}^{(0)} \rangle, \quad (10)$$

where $\epsilon_{\alpha\beta\gamma}$ is the Levi-Civita symbol, $nn(k)$ indicates nearest neighbors of the k -th atom, m_e is the electron rest mass, $r_{kk''}^{(\beta)}$ is the β component of the distance between atoms k and k'' , $r^{(\gamma)}$ is the γ component of the position operator, and H_0 is the tight-binding Hamiltonian. In the present tight-binding description that is augmented for optical properties, the matrix elements of $r^{(\gamma)}$ are obtained from the empirical transition dipole matrix elements.¹³ We have calculated the effect of this correction on the g factor for all dots and rods. In no case did it make a difference of more than 10^{-5} in the g factor. Since this is beyond the inherent accuracy of tight-binding, we conclude that this contribution may be omitted, substantially reducing the computational cost.

C. Electron g tensor for a pair of electrons in separate levels

In the case of neutral, undoped nanocrystals, unpaired spin (leading to a measurable electron spin resonance (ESR) signal) is caused by the creation of an exciton. It is often stated that in a particular NC, one may observe either an electron g factor due to only the conduction band electron as a result of rapid hole dephasing, or else a single g factor that results from exciton precession.^{4,24} The hole is assumed not to precess and its g factor is used as a fitting parameter in the effective mass expression for the exciton g factor.⁴ The electron g factor in this situation is to a first approximation, the same as the conduction electron g factor calculated in the previous section.

However, there is also the possibility, analogous to molecular ESR, in which an electron g factor is observed which is due to multiple unpaired electrons. For an arbitrary number of unpaired spins in single-electron levels p , having total spin S , Eq.(3) becomes¹⁶

$$g_{ij} = g_0 \delta_{ij} + \frac{1}{S} \sum_p \sum_{n \neq p} \sum_k \frac{\langle \psi_p | \xi_k(r_k) \mathbf{I}_k^i | \psi_n \rangle \langle \psi_n | \mathbf{I}_k^j | \psi_p \rangle}{E_p - E_n}. \quad (11)$$

Only the electron configuration of highest multiplicity is observed in ESR (and thus treated here), since the others have non-zero electric dipole matrix elements with lower multiplicity configurations. In our case, this corresponds to the $S = 1$ triplet (“dark”) exciton-like state, with neglect of electron-hole correlation.

We remark that this approach is not generally applicable to the treatment of the exciton g factor. In general, one needs to consider the effect of the magnetic field on the total angular momentum $J = L + S$ of the particle. However, in the n -doped case our state is a nondegenerate doublet ground state and as such may be represented by a real wavefunction; as a result $\langle L \rangle = 0$, allowing us to perform the treatment above. This does not hold if one considers mixing with excited electronic configurations. Taking into account the effect of magnetic field on J with a non-perturbative treatment of H_{spin} leads to similar trends in the anisotropy, however with significantly lower magnitude of electron g -factors, in better quantitative agreement with experiment. [P. C. Chen and K. B. Whaley, to be published.]

III. RESULTS

A. Building Nanocrystals

The crystal structures used here for the dots are the same as those used in previous tight-binding studies.^{9,13} These crystals are faceted with C_{3v} symmetry. They incorporate ligand effects through a semiempirical oxygen-like “atom” that fully saturates the cadmium surface sites. The surface selenium atoms possess dangling bonds. A set of calibration calculations that removed the dangling bonds, *i.e.*, truncated the surface Se atoms, was also performed in order to provide some assessment of the effect of dangling bonds on the magnitude of the g factors. To construct the nanocrystal rods, we used the largest dot as a template for the crystal structure, and then removed successive layers of the sides parallel to the non-wurtzite axes in order to arrive at the desired rod diameter. Surface ligands were added using the hydrogen-addition function in PC Spartan 2002, and then the Cd-ligand bond lengths were

lengthened to 2.625 Å using a perl script. Two series of rods were studied, possessing smaller or larger cross-sections. The first (smaller) series has diameter 21.4 Å × 24.79 Å, and the second (larger) series has diameter 32.3 Å × 45.5 Å. Note that since the crystal is in fact hexagonal, two dimensions are required to completely specify the cross-section of each rod, although we shall loosely distinguish the two series by their effective “diameters”. In both series, the shorter rods were created by removing two planes (of total width 3.5 Å) of atoms perpendicular to the wurtzite axis, in addition to the removal of layers from the sides parallel to this axis. This additional removal was necessary to keep the surface characteristics similar on all rod surfaces. This procedure for creating rods removes the C_{3v} symmetry of the nanocrystals, but does result in faceted rods possessing shapes that are qualitatively in agreement with the shapes characterized experimentally by transmission electron microscopy.²⁵ Additionally, in order to lengthen the rods, the structure of the preceding 7.0 Å in the wurtzite axis direction was duplicated and translated. Figure 1 shows cross-sections for the two series of rods employed here. Cross-sections of the C_{3v} symmetry dots are shown in Ref. 13.

B. n -doped systems

1. Dots

We calculated the g tensor for n -doped dots with diameters ranging from approximately 17 Å - 50 Å. Note that since these calculations are atomistic, the dots are faceted and are therefore only approximately spherical. The effective sphericity is given in Ref. 13. The g factor results for oxygen-passivated nanocrystals are shown in Figure 2a. We found the g factors to be relatively size-independent, and to possess average g factor values of ~ 2 . We have determined values for the anisotropic components as $g_{\parallel} \simeq 2.010$ and $g_{\perp} \simeq 2.004$. These components are identified by their degeneracy, with g_{\perp} being two-fold degenerate, and g_{\parallel} being singly degenerate. This small value of anisotropy would be extremely difficult to resolve experimentally, and the near-spherical shape dots are thus expected to appear “isotropic”.

2. Rods

We calculated the g tensor for n -doped rods of diameters 32.3 Å × 45.5 Å and 21.4 Å × 24.79 Å for various lengths, shown in Figures 2b and 2c-d, respectively. We found that in both cases the g factor changes abruptly when the length of the rod is approximately 1.3 times the diameter. The anisotropic components in both cases experienced a similar discontinuity. For the smaller diameter (21.4 Å × 24.79 Å) rod, the discontinuity is between $g_{iso} = 1.998 \pm 0.023$ (from 14.0 Å - 28.0 Å) and $g_{iso} = 1.913 \pm 0.020$ (from 31.5 Å - 45.5 Å), or $\Delta g_{iso} = 0.085 \pm 0.043$ between the 28.0 Å and 31.5 Å crystals. This region is shown as an inset in Figure 2c. Note that since this is a discrete atomistic treatment, we cannot “cut” the crystal at distances less than the 3.5 Å spacing. For the larger diameter (32.3 Å × 45.5 Å) rod, we calculated $\Delta g_{iso} = 0.3$, with the discontinuity in the isotropic g factor at approximately 1.3 times the smaller dimension of the diameter (between 38.5 Å and 42.0 Å). Since this dot-rod transition discontinuity is at least an order of magnitude greater than the TRFR resolution,^{4,5} it should be possible to measure this effect and could provide a useful method of examining aspect ratios during nano-rod synthesis. Furthermore, it is worth noting the large deviation from the free electron g factor and large g anisotropy that is possible by manipulation of shape alone, as demonstrated in the highly elliptical dots (Figures 2b and 2c). In the case of the larger rods, we observe that the g factor is anisotropic for the dot-like structures, then becomes essentially isotropic for crystals between the length of 42 Å to 71 Å, and then becomes anisotropic again for longer rod structures. This appears to bound the isotropically quasispherical region between aspect ratios 1.3 – 2. In the case of the smaller rods, both the isotropic and anisotropic components experience large changes as a function of size. This is to be expected when making a size study of small structures based on an atomistic model, since adding a layer of atoms to a small system provides a large perturbation of shape.

C. Neutral Systems

1. Dots

We evaluated the g factor for an electronic configuration with parallel spin electrons in conduction and valence band edge states (which we will refer to as the “excitonic electron” g factor) for each of the dot sizes treated in

Section IIIB1 using the approach discussed in Section IIC. Examining the results in Figure 3a, the largest of the dots treated theoretically here is comparable to the smallest dot treated experimentally, but there is no quantitative agreement with the experimentally measured g factors of 1.63 ± 0.01 and 1.565 ± 0.002 , 1.83 ± 0.01 for the 40 Å and 50 Å diameter dots, respectively.^{2,4,5} However, qualitatively, we note that there are no anisotropies larger than a factor of approximately 0.1.

2. Rods

The excitonic electron g factors for the rods treated in Section IIIB2 are shown in Figures 3b and 3c. The discontinuity at aspect ratio 1.3 is still present but is reduced by an order of magnitude for both rod sizes as compared to the n -doped electron g factor. However, the presence of an isotropically quasi-spherical region is the same for the electron in the excitonic system as for the n -doped electron g factor.

D. Truncated Surface Calculations

Surface reconstruction is an important factor in the optical spectroscopy of small NCs.¹⁴ One result of surface reconstruction for CdSe nanocrystals passivated by oxygen ligands is to move the Se dangling bonds away from the band edge to lower energies. To a first approximation, this can be modeled by removing the dangling selenium bonds on the surface of the NC. To ascertain the qualitative effect of surface reconstruction on our results, we performed the calculations for truncated nanocrystals without the dangling selenium bonds. Results are shown in Figures 4 and 5 for the n -doped electron and excitonic electron respectively.

Overall, we found the effect of surface truncation to be a decrease in magnitude of the g factor. For dots and for the $32.3 \text{ Å} \times 45.5 \text{ Å}$ diameter rods, the behaviour of the g factor components is qualitatively similar for both dangling and non-dangling cases. The apparent degeneracy of two of the g components in the dangling bond calculations (Figures 2b and 3b) is broken in the truncated calculations (Figures 4b and 5b). For the smaller, $21.4 \text{ Å} \times 24.79 \text{ Å}$ diameter rods, (Figures 4c and 5c) the behavior of the g components for surface truncated systems is qualitatively different. In particular, the g factor becomes isotropic at aspect ratio ~ 3 for both the n -doped (Figure 4c) and excitonic (Figure 5c) electron g factors. Since one would expect the smaller crystals to show a more profound change due to their larger surface area to volume ratio, it is not entirely surprising that the behavior of small rods deviates from that of larger rods. The results suggest that surface reconstruction is an important effect for the g factors of small nanocrystals in both quantitative and qualitative terms, and warrants more detailed investigation.

E. Orbital Character

To examine the origin of the discontinuity in the g factor at aspect ratio 1.3, the appearance of isotropic regions, and the general qualitative behavior of g , we examined the character of the near band-edge orbitals. For the conduction band edge state and nine states above as well as the valence band edge state and nine states below, we calculated the fractional contribution of the various types of atomic orbitals to the given molecular orbital. The results for the $32.3 \text{ Å} \times 45.5 \text{ Å}$ rod are shown in Figure 6. The left panels show the orbital contributions with the inclusion of dangling Se surface bonds, and the right panels show the results from truncated nanocrystals with the dangling Se bonds removed. Shown within each figure are graphs for the orbital contributions where the maximum fractional content exceeded 0.15. Dotted lines depict the the conduction band edge and higher states, and solid lines depict the valence band edge and lower states.

Qualitatively, the fractional orbital content of the conduction and valence band edge states behave similarly for both types of surface treatments. There is an increase in the Cd- s contribution at aspect ratio ≈ 1.3 , which then decreases at aspect ratio 2.5, corresponding to a simultaneous decrease of the Se- p contributions. While the behavior of the valence and conduction band edge states themselves are relatively unaffected by the surface treatment, truncating the dangling Se surface bonds appears to be a reduction in the Se- p content for the other states. This is not surprising, in light of the similarity between the g factor behavior for the dangling and truncated calculations.

Results for the smaller rods are more complicated, and are not shown. Although the Cd- s atomic orbital contribution is similar for both surface treatments, the Se- p level is qualitatively different.

IV. DISCUSSION

A. Shape-Controlled g factor Discontinuity

1. Relation to HOMO/LUMO Wavefunction

The result concerning the discontinuity in the g factor for CdSe rods at the 1.3 aspect ratio suggests that small size differences in the growth axis length can have large effects on both the magnitude and the anisotropy of the g factor. An examination of CdSe rods using the semiempirical pseudopotential method by Hu *et al.*²⁶ studied changes in the electronic states as a function of rod length. In particular, level crossing occurs between the two highest occupied orbitals (i.e., the HOMO and the level below it, HOMO-1) at an aspect ratio of ~ 1.3 , and of the HOMO-4 and HOMO-5 levels at an aspect ratio of ~ 2 . In each case this level crossing involved a change in relative contributions of Se $4p_z$ and Se $4p_{x,y}$ levels, matching linearly polarized emission spectroscopic results.²⁷ We observe qualitative agreement with these results, as discussed in Section III E. However, since the pseudopotential study of Hu *et al.*, does not include surface reconstruction effects, the details for small nanocrystals may differ. It is obvious, however, that these changes in the orbital arrangement will have a large effect on the g factor, as it is dependent on the orbital angular momentum of the state in question.

Additionally, we have performed calculations in which we turned off the wurtzite crystal field correction in our non-truncated surface calculations to assess the role of the crystal symmetry on the g factor discontinuity. For both rods, this resulted in splitting the approximately degenerate g levels in the regions outside of the range of aspect ratio $1.3 - 2$, but the existence of an isotropic region as well as the discontinuity in the isotropic g factor persisted. This suggests that the discontinuity and isotropic region that we observe are shape effects, rather than simply a cancellation of the wurtzite crystal field, as proposed in the “quasi-spherical” model.⁴

2. Connection to Experimental Observation of Multiple g factors

We conjecture that this discontinuity effect may play a role in the existence of four g factors in the experiments on 57-Å radius quantum dots. This size dot is unique in showing four g factors: both slightly smaller and larger dots display only two.^{2,4,5} It is well known that the so-called “dots” are in fact elliptical; empirically observed relations for the ellipticity of quantum dots as a function of size, based on transmission electron microscopy data, give an aspect ratio of ~ 1.34 for the 57-Å dot, whereas other dots have either smaller or larger aspect ratios.^{4,13,28} Since the size control is on the order of $\pm 5\%$, this suggests that unlike the other samples studied, the size distribution of the 57-Å dot may in fact span the discontinuity we observe here. We have tabulated the dot size, number of g factor components observed, and aspect ratios in Table I. This suggests two possible situations that may give rise to four g components. The first scenario assigns the components as resulting from an exciton and an isotropic electron component (as assigned in effective mass studies^{4,5}) deriving from the portion of the NC ensemble in the isotropically quasispherical region, plus two anisotropic electron components from the lower aspect ratio portion of the ensemble. The second possible assignment arises from one electron g factor and one exciton g factor on either side of the discontinuity. It is our hope that this analysis will encourage TRFR experiments on even more precisely size selected nanocrystal samples, as well as on n -doped nanocrystalline systems, in order to distinguish between these assignments.

B. Extensions

There are several limitations of this study. The first is due to the use of a sp^3s^* semiempirical basis. In particular, the s^* orbital was introduced by Vogl *et al.* with the intent of mimicking d -orbitals.²⁹ While satisfactory for optical calculations, this orbital has no angular momentum, since $l = 0$ for s^* , as opposed to $l = 2$ for d . To go beyond this initial analysis, one might have to include d -orbitals (i.e., use a sp^3d^5 or $sp^3d^5s^*$ tight-binding basis) or else to include angular momentum for the s^* orbital empirically. Additionally, it is not clear that the semiempirical basis accurately corresponds to the eigenfunctions of angular-momentum that we attribute to it via s , p , etc., labels. Second, the ligand model treats oxygen as an s -orbital only, neglecting any angular momentum contributions. As mentioned in Section II B, this is partially justifiable by the much smaller spin-orbit coupling of oxygen compared to Cd or Se. However, for small crystals we expect this may fail, since the ratio of ligands to semiconductor atoms increases. Again, it may be necessary to include a larger basis (i.e., p -orbitals on the oxygen atoms) or to determine an empirical correction to account for this effect. Third, while we found the correction to Stone’s second approximation, Eq.(10), to be negligible,

this is dependent on the validity of the transition dipole matrix elements, which were empirically devised to reproduce optical spectra,¹³ and as a result may not be applicable to magneto-optical problems. Fourth, the neglect of off-site terms in the evaluation of the angular-momentum matrix elements (Eqs. 7, 8) further decreases the magnitude of the shift from the free-electron g factor. If a more quantitative analysis were desired, one could directly parameterize these angular-momentum matrix elements by fitting to bulk or to ab initio calculations of the g factor in small clusters. To our knowledge, the latter has not been performed for CdSe, although there exist separate studies of density functional theory (DFT) calculations on CdSe clusters of sizes up to ~ 200 atoms³⁰ as well as methods to calculate the g tensor using DFT³¹. Finally, while treating the spin Hamiltonian perturbatively is satisfactory in organic and organometallic molecules,^[cite: 23] this approximation may not be as appropriate for the quantitative description of semiconductor systems, due to the larger spin-orbit coupling constants. Nevertheless, the qualitative trends with respect to shape observed here do also appear to hold when the spin Hamiltonian is treated non-perturbatively. [P. C. Chen and K. B. Whaley, to be published.]

The issue of surface effects is complicated by the shape dependence of the g factor. To proceed in future work, it may be most effective to decouple these two effects. To examine the effect of shape alone (ignoring surface reconstruction effects), one may modify the existing effective mass treatments of the g factor in spherical nanocrystals to treat rods. This would have the added benefit of being able to treat the larger experimental nanocrystal sizes, in particular the 57 Å dot, to test whether the discontinuity in the g factor at aspect ratio 1.3 is present for larger size crystals. Second, since we have seen indications that surface reconstruction may have substantial qualitative effects on the behavior of the g factor in small nanocrystals, one may apply the tight-binding surface reconstruction method (via total energy minimization) previously applied to CdSe nanocrystals,⁹ in order to resolve the differences between the dangling Se-bond and truncated surface calculations, and to determine whether this plays a role in why the smallest dot studied in TRFR experiments shows only one g factor component.^{4,5}

V. SUMMARY

We have developed a tight-binding theory for the Lande g tensor for electrons in n -doped and excitonic systems, which we have applied to CdSe quantum dots and rods. For n -doped systems, we found the electron g factor for approximately spherical dots to be independent of dot size, while a discontinuity in the g factor appears as the c -axis is extended to form rod-like structures. Similar behavior is observed for excitonic electrons, although the magnitude of both the g factor and its discontinuity was found to be dependent on the treatment of dangling surface Se bonds. We also observe the existence of an isotropically quasispherical regime between aspect ratio 1.3 – 2 in all cases. This appears to correspond to the “quasi-spherical hypothesis” suggested in the effective mass treatments of the g factor.⁴ However, whereas the previous treatments consider this as arising from the cancellation of wurtzite crystal field effects on g by shape terms, the isotropic region we observe here appears to be due primarily to shape effects, and occurs even in the absence of the wurtzite crystal field. Comparison with available experimental TRFR data indicates that the discontinuity between the anisotropic and isotropic regions offers a possible explanation for multiple g factors.

Note Added in Proof. An effective mass treatment for rod-shaped wurtzite nanocrystals has recently been presented by Li and Xia, but the method has not yet been applied to the calculation of g factors. [cite: X.-Z. Li and J.-B. Xia, Phys. Rev. B. **66**, 115316 (2002)].

VI. ACKNOWLEDGEMENTS

We would like to thank Kenneth Brown for many insightful conversations. J.S. thanks the National Defense Science and Engineering Grant (NDSEG) program and U.S. Army Research Office Contract/Grant No. FDDAAD19-01-1-0612 for financial support. K.B.W. thanks the Miller Institute for Basic Research in Science for financial support. This work was also supported by the Defense Advanced Research Projects Agency (DARPA) and the Office of Naval Research under Grant No. FDN00014-01-1-0826.

¹ D. D. Awschalom and J. M. Kikkawa, Physics Today **52**, 33 (1999).

² J. A. Gupta, D. D. Awschalom, X. Peng, and A. P. Alivisatos, Phys. Rev. B **59**, R10421 (1999).

³ S. A. Wolf, D. D. Awschalom, R. A. Buhrmanand, J. M. Daughton, S. von Molnar, M. L. Roukes, A. Y. Chtchelkanova, and D. M. Treger, Science **294**, 1488 (2001).

⁴ J. A. Gupta, D. D. Awschalom, A. L. Efros, and A. V. Rodina, Phys. Rev. B **66**, 125307 (2002).

⁵ J. A. Gupta, Ph.D. thesis, University of California, Santa Barbara (2002).

- ⁶ M. Kuno, M. Nirmal, M. G. Bawendi, A. Efros, and M. Rosen, *J. Chem. Phys.* **108**, 4242 (1998).
- ⁷ E. Johnston-Halperin, D. D. Awschalom, S. A. Crooker, A. L. Efros, M. Rosen, X. Peng, and A. P. Alivisatos, *Phys. Rev. B* **63**, 205309 (2001).
- ⁸ A. A. Kiselev, K. W. Kim, and E. L. Ivchenko, *Phys. Stat. Sol. B* **215**, 235 (1999).
- ⁹ S. Pokrant and K. B. Whaley, *Eur. Phys. J. D* **6**, 255 (1999).
- ¹⁰ L. Manna, E. C. Scher, and A. P. Alivisatos, *J. Am. Chem. Soc.* **122**, 12700 (2000).
- ¹¹ M. Shim and P. Guyot-Sionnest, *Nature* **407**, 981 (2000).
- ¹² C. Wang, M. Shim, and P. Guyot-Sionnest, *Science* **291**, 2390 (2001).
- ¹³ K. Leung, S. Pokrant, and K. B. Whaley, *Phys. Rev. B* **57**, 12291 (1998).
- ¹⁴ K. Leung and K. B. Whaley, *J. Chem. Phys.* **110**, 11012 (1999).
- ¹⁵ P. E. Lippens and M. Lannoo, *Phys. Rev. B* **41**, 6079 (1990).
- ¹⁶ A. J. Stone, *Proc. Roy. Soc. A* **271**, 424 (1963).
- ¹⁷ C. P. Keijzers, H. J. M. de Vries, and A. van der Avoird, *Inorg. Chem.* **11**, 1338 (1972).
- ¹⁸ B. F. Minaev, *Opt. Spektrosk.* **36**, 275 (1974).
- ¹⁹ D. J. Chadi, *Phys. Rev. B* **16**, 790 (1977).
- ²⁰ J. R. Morton, J. R. Rowlands, and D. H. Whiffen, *Atomic properties for interpreting ESR data* (1962), National Physical Laboratory – BPR 13.
- ²¹ J. T. Törring, S. Un, M. Knüpling, M. Plato, and K. Möbius, *J. Chem. Phys.* **107**, 3905 (1997).
- ²² Y.-W. Hsiao and M. C. Zerner, *Int. J. Quantum Chem.* **75**, 577 (1999).
- ²³ P. J. Bratt, O. G. Poluektov, M. C. Thurnauer, J. Krzystek, L.-C. Brunel, J. Schrier, Y.-W. Hsiao, M. Zerner, and A. Angerhofer, *J. Phys. Chem. B* **104**, 6973 (2000).
- ²⁴ A. V. Rodina, A. L. Efros, M. Rosen, and B. K. Meyer, *Mat. Sci. Eng. C* **19**, 435 (2002).
- ²⁵ A. C. Carter, C. E. Bouldin, K. M. Kemmer, M. I. Bell, J. C. Woicik, and S. A. Majetich, *Phys. Rev. B* **55**, 13822 (1997).
- ²⁶ J. Hu, L.-W. Wang, L.-S. Li, W. Yang, and A. P. Alivisatos, *J. Phys. Chem. B* **106**, 2447 (2002).
- ²⁷ J. Hu, L. S. Li, W. D. Yang, L. Manna, L. W. Wang, and A. P. Alivisatos, *Science* **292**, 2060 (2001).
- ²⁸ A. V. Kadavanich, Ph.D. thesis, University of California, Berkeley (1997).
- ²⁹ P. Vogl, H. P. Hjalmarson, and J. D. Dow, *J. Phys. Chem. Solids* **44**, 365 (1983).
- ³⁰ M. C. Tropicovsky, L. Kronik, and J. R. Chelikowsky, *Phys. Rev. B* **65**, 033311 (2001).
- ³¹ S. Patchkovskii and T. Ziegler, *J. Phys. Chem. A* **105**, 5490 (2001).

TABLE I: Number of g factor components observed in TRFR experiments^{2,4} as a function of nanocrystal effective radius and aspect ratio. For the 22 Å and 25 Å dots we use the sixth-order polynomial fit to aspect ratio described in Ref. 13; for the 40 Å and 50 Å dots we use the linear fit described in Ref. 28; for the 80 Å dot we use the aspect ratio given in Ref. 4.

Effective Radius (Å)	Aspect Ratio	g components
22	1.17	1
25	1.20	2
40	1.23	2
57	1.34	4
80	2	2

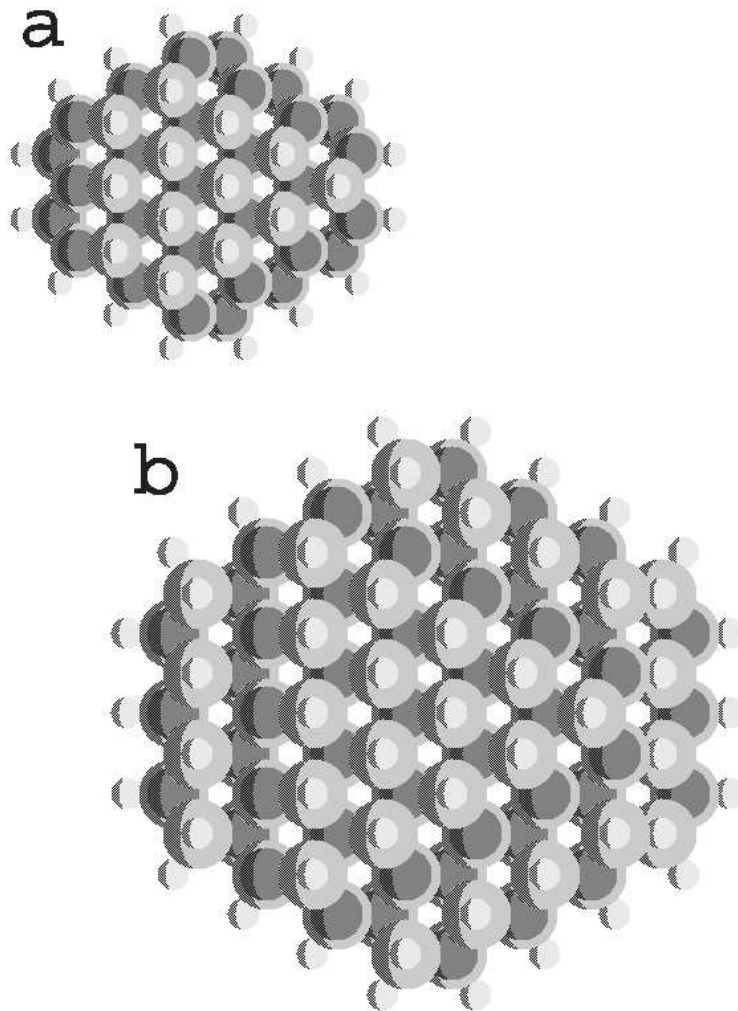


FIG. 1: Cross section of nanocrystal rods. Small circles are ligand atoms. Large light circles are Cd atoms, and medium dark circles are Se atoms. a) Cross section of 21.4 Å × 24.79 Å (small) rod. b) Cross section of 32.3 Å × 45.5 Å (large) rod.

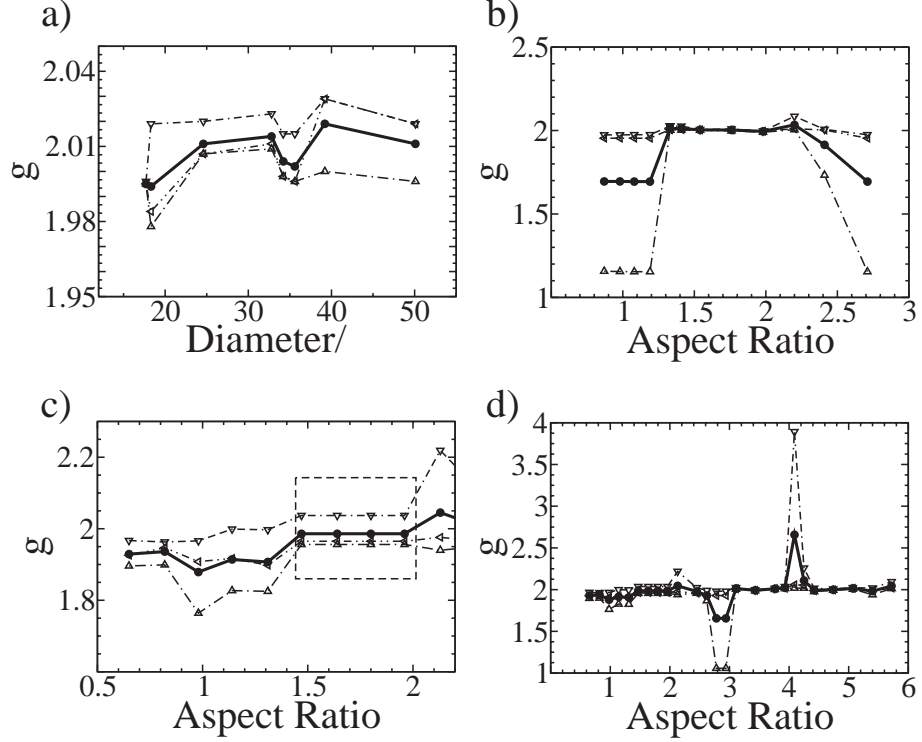


FIG. 2: Conduction electron g factors for the n -doped CdSe nanocrystals. In all figures, dashed lines with open symbols represent the three anisotropic components of the g tensor, and the solid line with filled circles represents the geometric mean (“isotropic” g factor) of the components. a) n -doped dot g factors as a function of dot diameter in Angstroms; the number of atoms varies from 96 to 1783. b) $32.3 \text{ \AA} \times 45.5 \text{ \AA}$ cross-section n -doped rod g factors as a function of aspect ratio; the number of atoms varies from 705 to 2252. Note the clear discontinuity in the g factor at aspect ratio ~ 1.3 , and the quasi-spherical region extending between aspect ratio 1.3 and 2. c) $21.4 \text{ \AA} \times 24.79 \text{ \AA}$ cross-section n -doped rod g factors as a function of aspect ratio; the number of atoms varies from 197 to 651. Note the jump in the g factor $\Delta g_{iso} \sim 0.1$ at aspect ratio ~ 1.3 and the quasi-spherical region (shown in dashed box). d) $21.4 \text{ \AA} \times 24.79 \text{ \AA}$ cross section n -doped rod g factors over a longer range of aspect ratios; the number of atoms varies from 197 to 1773.

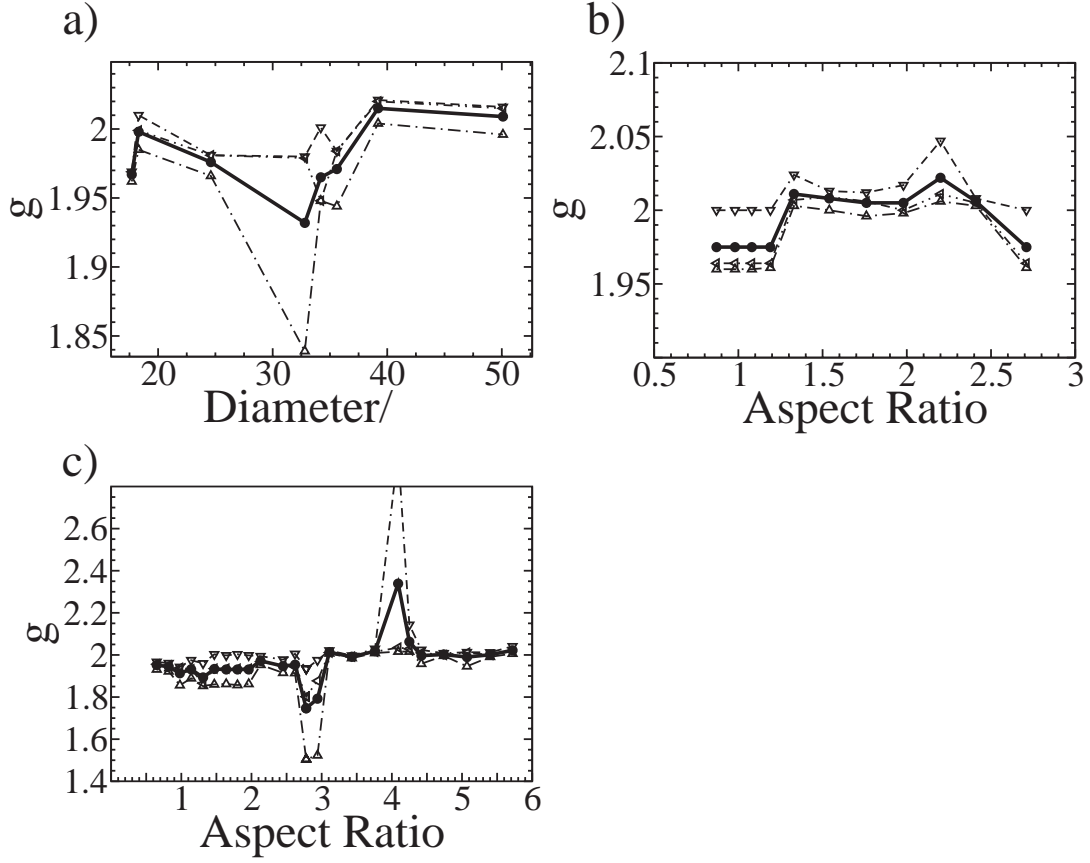


FIG. 3: g factors in CdSe nanocrystals, calculated for electronic configurations having two unpaired electrons with parallel spin in valence and conduction band edge states. In all figures, dashed lines with open symbols represent the three anisotropic components of the g tensor, and the solid line with filled circles represents the geometric mean ("isotropic" g factor) of the components. See caption of Figure 2 for corresponding number of atoms. Comparing to the previous figure, the qualitative behavior is similar in all cases. a) Dots. b) $32.3 \text{ \AA} \times 45.5 \text{ \AA}$ cross-section rods. Note that while the qualitative behavior is similar, the magnitude of the g factor discontinuity is reduced by an order of magnitude. c) $21.4 \text{ \AA} \times 24.79 \text{ \AA}$ cross-section rods over a larger range of aspect ratios.

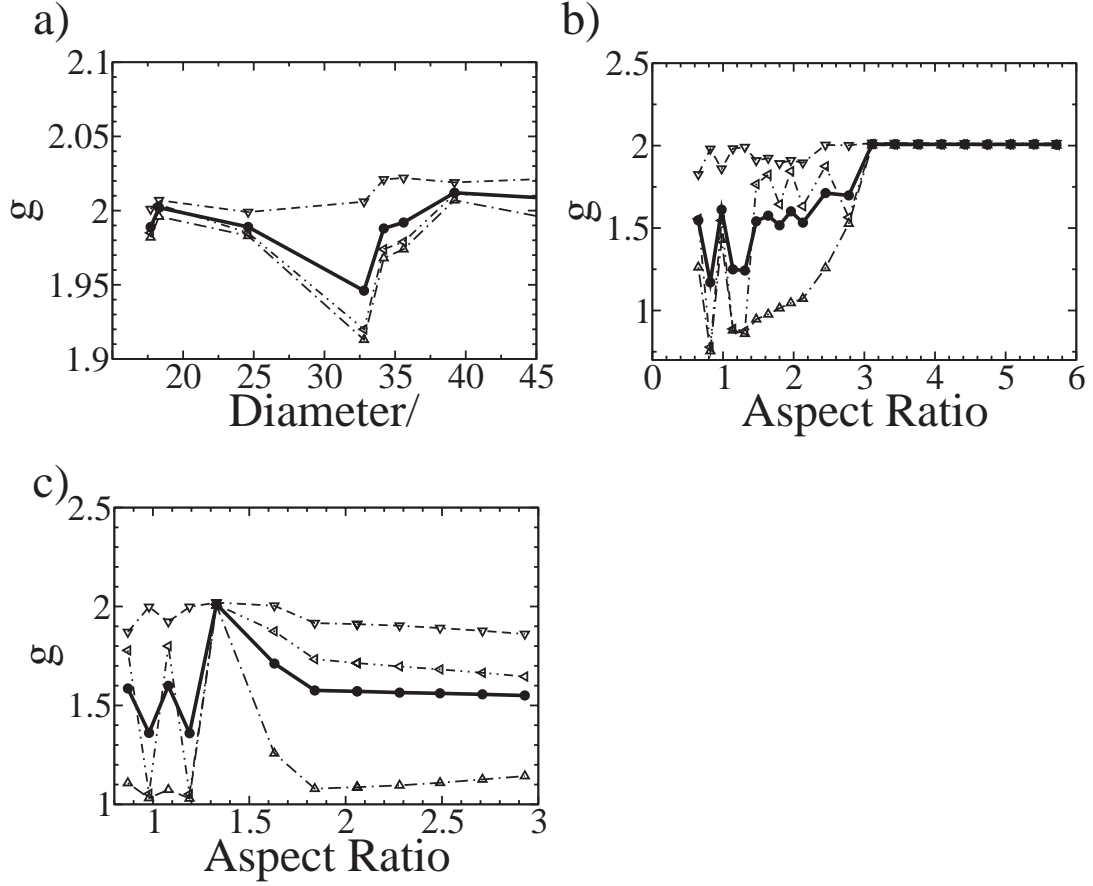


FIG. 4: Conduction electron g factors for n -doped CdSe nanocrystals with Se dangling bonds truncated. In all figures, dashed lines with open symbols represent the three anisotropic components of the g tensor, and the solid line with filled circles represents the geometric mean ("isotropic" g factor) of the components. See caption of Figure 2 for corresponding number of atoms. a) Dots. The decrease in the g factor magnitudes for the 35 Å diameter dots is increased as compared to the dangling bond calculations, but the overall qualitative behavior is unchanged. b) $32.3 \text{ \AA} \times 45.5 \text{ \AA}$ cross-section rods. Note the abrupt change at aspect ratio ~ 1.3 , but the lack of an isotropic behavior between aspect ratios 1.3–2 as seen in the dangling bond calculation in Figure 2b. c) $21.4 \text{ \AA} \times 24.79 \text{ \AA}$ cross-section rods. These small rods show qualitatively different behavior, with the g factor becoming isotropic at significantly larger aspect ratios, greater than ~ 3 .

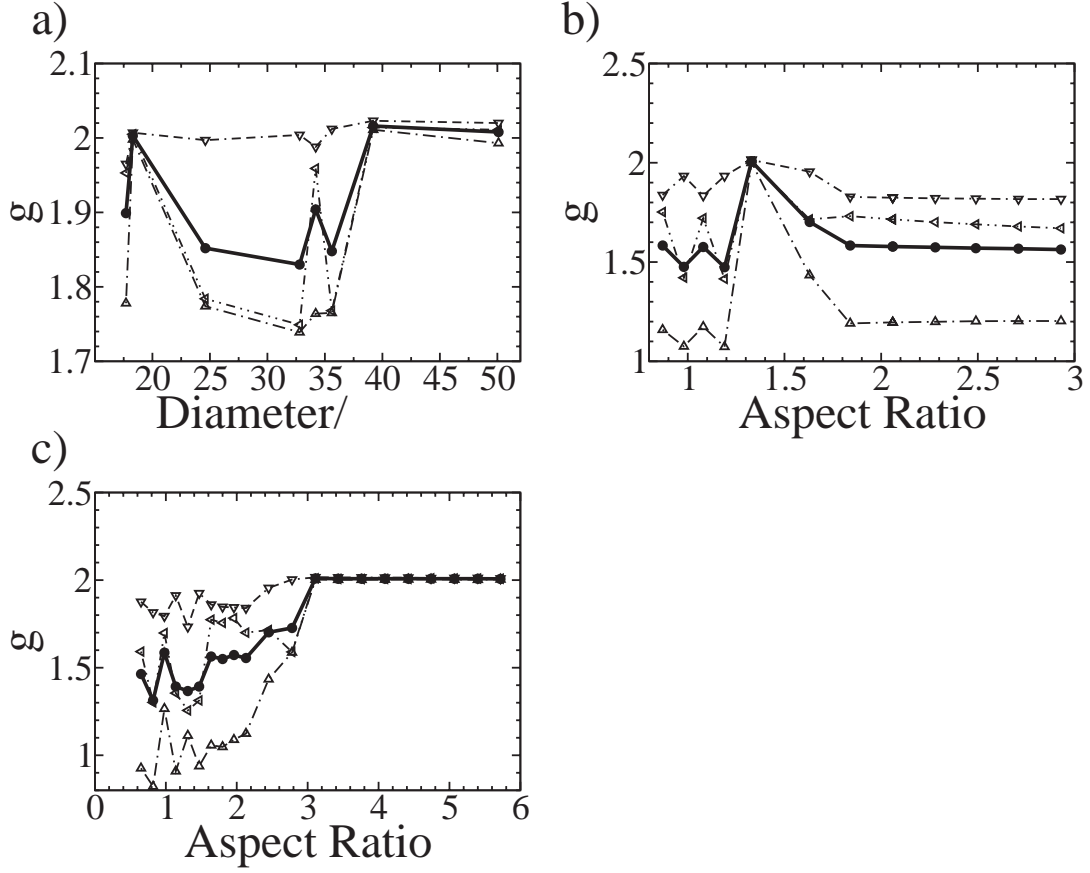


FIG. 5: g factors for neutral CdSe nanocrystals with Se dangling bonds truncated. All calculations are made for electronic configurations having two unpaired electrons with parallel spin in valence and conduction band edge states. In all figures, dashed lines with open symbols represent the three anisotropic components of the g tensor, and the solid line with filled circles represents the geometric mean ("isotropic" g factor) of the components. See caption of Figure 2 for corresponding number of atoms. a) Dots. b) $32.3 \text{ \AA} \times 45.5 \text{ \AA}$ cross-section rods. c) $21.4 \text{ \AA} \times 24.79 \text{ \AA}$ cross-section rods. Note in all cases the qualitative similarity to the conduction band electron g factors shown in Figure 4.

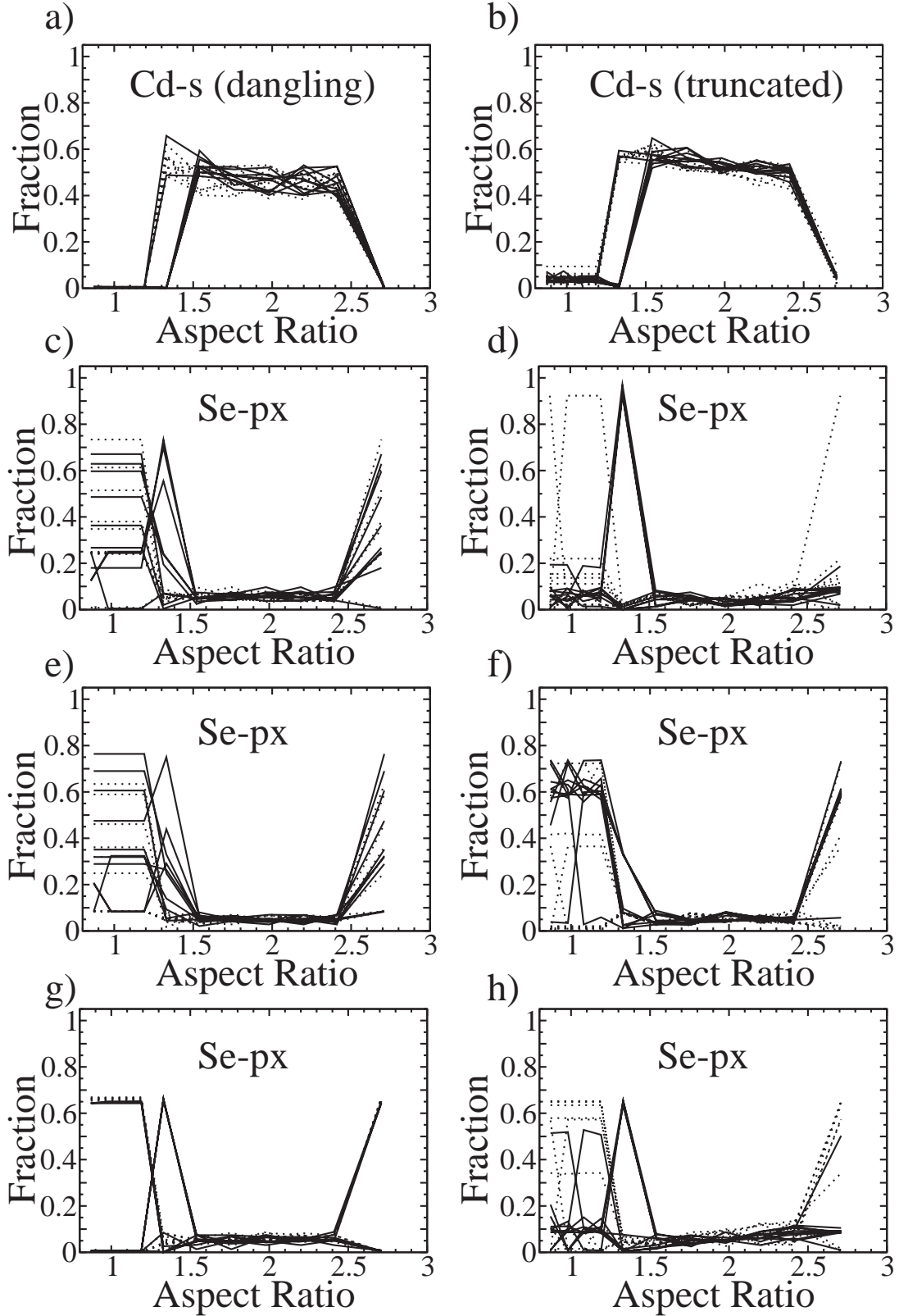


FIG. 6: Fractional atomic-orbital contents for the $32.3 \text{ \AA} \times 45.5 \text{ \AA}$ cross-section CdSe nanocrystal rods, as a function of aspect ratio. The number of atoms varies from 705 to 2252. Dotted lines depict the content of the conduction band edge and the 9 levels above; solid lines depict the content of the valence band edge and the 9 levels below. Orbital types where the maximum fractional content was less than 0.15 are omitted. Left column panels are with the inclusion of Se dangling bonds, right column panels truncate Se dangling bonds.